

Epimorphin deletion protects mice from inflammation-induced colon carcinogenesis and alters stem cell niche myofibroblast secretion

Anisa Shaker,¹ Elzbieta A. Swietlicki,¹ Lihua Wang,¹ Shujun Jiang,¹ Birce Onal,¹ Shashi Bala,¹ Katherine DeSchryver,¹ Rodney Newberry,¹ Marc S. Levin,^{1,2} and Deborah C. Rubin^{1,3}

¹Department of Internal Medicine, Washington University School of Medicine, Saint Louis, Missouri, USA. ²Department of Medicine, Saint Louis VA Medical Center, Saint Louis, Missouri, USA. ³Department of Developmental Biology, Washington University School of Medicine, Saint Louis, Missouri, USA.

Epithelial-mesenchymal interactions regulate normal gut epithelial homeostasis and have a putative role in inflammatory bowel disease and colon cancer pathogenesis. Epimorphin is a mesenchymal and myofibroblast protein with antiproliferative, promorphogenic effects in intestinal epithelium. We previously showed that deletion of epimorphin partially protects mice from acute colitis, associated with an increase in crypt cell proliferation. Here we explored the potential therapeutic utility of modulating epimorphin expression by examining the effects of epimorphin deletion on chronic inflammation-associated colon carcinogenesis using the azoxymethane/dextran sodium sulfate (AOM/DSS) model. We found that mice in which epimorphin expression was absent had a marked reduction in incidence and extent of colonic dysplasia. Furthermore, epimorphin deletion in myofibroblasts altered the morphology and growth of cocultured epithelial cells. Loss of epimorphin affected secretion of soluble mesenchymal regulators of the stem cell niche such as Chordin. Importantly, IL-6 secretion from LPS-treated epimorphin-deficient myofibroblasts was completely inhibited, and stromal IL-6 expression was reduced in vivo. Taken together, these data show that epimorphin deletion inhibits chronic inflammation-associated colon carcinogenesis in mice, likely as a result of increased epithelial repair, decreased myofibroblast IL-6 secretion, and diminished IL-6-induced inflammation. Furthermore, we believe that modulation of epimorphin expression may have therapeutic benefits in appropriate clinical settings.

Introduction

Dynamic and reciprocal epithelial-mesenchymal interactions play a critical role in intestinal morphogenesis, maintenance of the steady state between epithelial proliferation and differentiation along the crypt villus axis (1), and epithelial carcinogenesis (2, 3). The gut mesenchyme, which gives rise to subepithelial myofibroblasts as well as other stromal components (4), supports the normal growth and development of the endoderm and directs regional specificity in the gut (1, 5, 6). Mesenchymal stem cells (MSCs) likely play an important role in epithelial injury and repair (7–9). Intestinal subepithelial myofibroblasts are located in the lamina propria and are directly adjacent to the crypts, which contain epithelial stem and proliferating progenitor cells. Myofibroblasts secrete a variety of signaling molecules, growth factors, and soluble mediators of inflammation. These cells play a critical role in epithelial restitution and wound repair and contribute to modulation of the immune response, tissue fibrosis, and colonic tumorigenesis (3, 8, 10).

Epimorphin is a mesenchymal/myofibroblast protein that is a member of the syntaxin family of membrane bound, intracellular vesicle docking proteins known as t-SNAREs (11–13). Monomeric epimorphin (also referred to as syntaxin 2) has been detected intracellularly as a component of the SNARE machinery that targets secretory vesicles to the plasma membrane (13, 14). Studies of

lung, skin, and mammary epithelium suggest a role for myofibroblast/stromal epimorphin in the formation of luminal, ductular, or branching structures during ontogeny (11, 15, 16). The molecular basis of the biologic function of epimorphin is complex, and investigations of its role in morphogenesis of the mammary epithelium have suggested that epimorphin has distinct, cell-specific extra- and intracellular roles (12, 16, 17).

We have previously shown that epimorphin is expressed by intestinal subepithelial myofibroblasts and that it exerts antiproliferative, promorphogenic effects on adjacent small intestinal epithelium (18). To precisely define its *in vivo* role, we generated epimorphin-deleted (*Epim*^{-/-}) mice and showed that epimorphin regulates basal proliferation of small intestinal, but not colonic, epithelium (19). Neonatal *Epim*^{-/-} mice have increased small bowel crypt depth, crypt cell proliferation, and crypt fission. The consequences of epimorphin deletion are mediated, at least in part, by effects on bone morphogenetic protein (BMP) and Wnt- β -catenin pathways (18, 19). Deletion of epimorphin partially protected the colon from injury in a dextran sodium sulfate-induced (DSS-induced) colitis model, associated with a marked increase in crypt cell proliferation (19). These studies suggested that effects of epimorphin deletion on downstream effector pathways may have potential therapeutic benefit for human inflammatory bowel disease (IBD). A critical complication of chronic gut inflammation from IBD is a markedly increased risk of colon cancer (20). To determine the long-term effect of epimorphin deletion in colitis-associated colon cancer, here

Conflict of interest: The authors have declared that no conflict of interest exists.

Citation for this article: *J Clin Invest.* 2010;120(6):2081–2093. doi:10.1172/JCI40676.

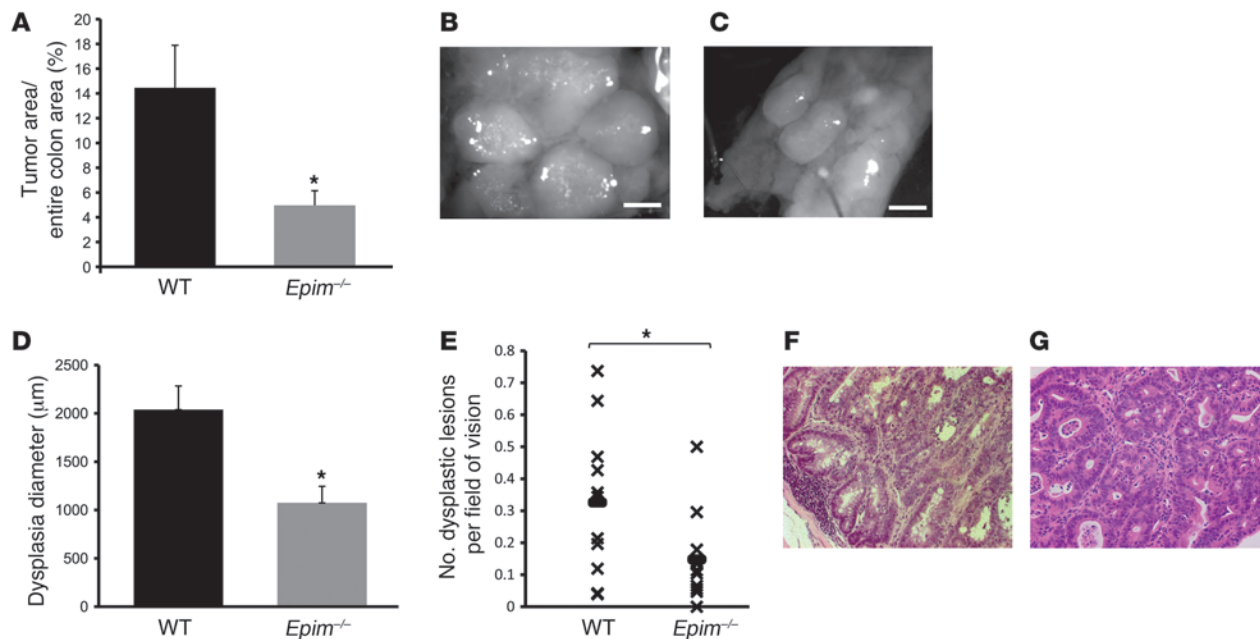


Figure 1 Protection from tumorigenesis in *Epim*^{-/-} mice. (A) Tumor load was decreased in AOM/DSS-treated *Epim*^{-/-} versus WT mice. Data are expressed as percent of total colonic surface area with tumor: WT, 14.45% (*n* = 11); *Epim*^{-/-}, 4.96% (*n* = 11). (B and C) Reduced polyposis in *Epim*^{-/-} compared with WT mice. (B) Polyps in WT mice coalesced together with minimal normal intervening colonic mucosa. (C) In contrast, polyps in *Epim*^{-/-} mice were separated by normal mucosa, and lesions had distinct boundaries. Scale bars: 625 µm. (D) Reduced dysplastic lesion diameter in *Epim*^{-/-} mice. Sections were stained with H&E, and the diameter of each area of dysplasia was measured: *Epim*^{-/-}, 1,075 µm (*n* = 11); WT, 2,040 µm (*n* = 11). (E) Reduced number of dysplastic lesions per field of vision in *Epim*^{-/-} mice: *Epim*^{-/-}, 0.15 (*n* = 11); WT, 0.33 (*n* = 11). (F and G) H&E staining of dysplastic mucosa from WT (F) and *Epim*^{-/-} (G) descending colon. Original magnification, ×200. **P* < 0.05.

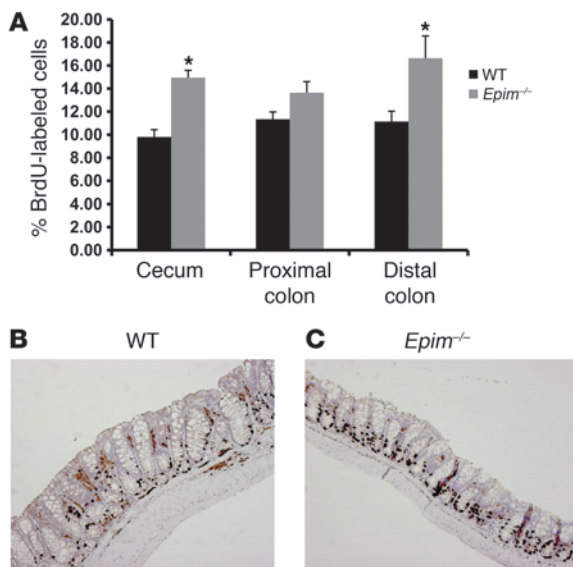
we examined the susceptibility of *Epim*^{-/-} mice to chronic inflammation-induced carcinogenesis using the azoxymethane/DSS (AOM/DSS) model. Epimorphin deletion resulted in an increase in colonic crypt cell proliferation, yet markedly reduced dysplastic tumor burden. Absence of epimorphin profoundly affected myofibroblast secretory function and response to LPS, resulting in altered myofibroblast interactions with epithelium, in an in vitro coculture model. In vivo analysis revealed decreased BMP signaling and reduced IL-6 expression in AOM/DSS-treated *Epim*^{-/-} colons. Our results suggest that the myofibroblast plays an important role in inflammation-induced colon cancer and that strategies to alter myofibroblast function may provide novel therapeutic avenues for the treatment of colitis and prevention of colitis-associated cancer.

Results

Epimorphin deletion markedly reduces dysplasia and polyposis in the AOM/DSS model of colon carcinogenesis. To determine the effects of epimorphin deletion on inflammation-induced dysplasia and carcinogenesis, we treated congenic *Epim*^{-/-} mice (C57BL/6J) and WT C57BL/6J mice with AOM (13.5 mg/kg) followed by 3 5-day cycles of 2.5%–3.0% DSS (Supplemental Figure 1; supplemental material available online with this article; doi:10.1172/JCI40676DS1). This regimen was chosen based on our pilot studies (see Methods) that showed that lower doses of AOM and DSS (21, 22) were ineffective in inducing dysplasia in WT and *Epim*^{-/-} mice. The higher doses resulted in dysplasia in 11 of 11 WT mice and 10 of 11 *Epim*^{-/-} mice, with a mortality rate of 50% (11 of 22) of WT mice and 35% (6 of 17) of *Epim*^{-/-} mice (*P* = NS).

Induction of colitis in mice results in body weight loss. The percent body weight loss in *Epim*^{-/-} mice was significantly reduced compared with WT mice after the completion of the second of 3 DSS treatments (Supplemental Figure 2).

The pattern and extent of polyposis was evaluated in all mice that survived the regimen (11 *Epim*^{-/-} and 11 WT). *Epim*^{-/-} mice had a markedly decreased tumor load, with a decrease in the percentage of total colonic surface area grossly replaced by tumor, compared with WT mice (WT, 14.45%; *Epim*^{-/-}, 4.96%; *P* = 0.01; Figure 1A). Whereas all WT mice had polyps and dysplasia, 1 of 11 *Epim*^{-/-} mice had no evidence of polyps and dysplasia. Polyposis in the WT mice was characterized grossly by multiple coalescing tumors with very small areas of intervening normal mucosa. In contrast, the *Epim*^{-/-} polyposis phenotype consisted of scattered lesions throughout the descending colon, separated by wide areas of normal mucosa (Figure 1, B and C). Histological analysis by H&E staining revealed that in addition to gross polyposis, there were also areas of “flat” dysplastic change. The diameter of each area of dysplasia per field of vision was measured by ocular micrometer. In the WT mouse colon, the average diameter of the dysplastic area was 2,040 µm compared with 1,075 µm in *Epim*^{-/-} mice (*P* < 0.01; Figure 1D). In addition, there was a decrease in the number of dysplastic lesions per field of vision in *Epim*^{-/-} mice (14.8%; *n* = 11) compared with WT mice (32.6%; *n* = 11; *P* = 0.041; Figure 1E). 1 of 11 *Epim*^{-/-} mice had dysplasia in the ascending colon in addition to the descending colon; 4 of 11 WT mice had dysplasia in the ascending colon or cecum in addition to the descending colon. There were no differences in the severity or grade of dys-



plasia comparing WT with *Epim*^{-/-} mice (Figure 1, F and G). In addition, the pattern of β-catenin immunostaining was similar, with nuclear accumulation only in areas of high-grade dysplasia (Supplemental Figure 3). Cyclin D1 expression was also similar (data not shown).

After brief exposure to DSS, *Epim*^{-/-} mice exhibited a marked increase in colonic crypt cell proliferation (19). AOM/DSS-treated mice were injected with 5-BrdU 90 minutes prior to sacrifice, and the labeling index was calculated in nondysplastic areas of the cecum and the proximal and distal colon (Figure 2). There was a significant increase in crypt cell proliferation in *Epim*^{-/-} versus WT mice in the cecum (*Epim*^{-/-}, 14.64%; WT, 9.11%; *P* < 0.005) and distal colon (*Epim*^{-/-}, 16.64%; WT, 11.15%; *P* = 0.051), with a trend toward an increase in the proximal colon. However, in dysplastic areas of descending colon, there were no differences in cellular proliferation per unit surface area (data not shown).

Areas of dysplastic and normal epithelium were evaluated for apoptotic rate. There was no change in apoptosis in *Epim*^{-/-} compared with WT mice, although effects on apoptosis at an earlier stage in the disease process cannot be ruled out, since tissues were analyzed at the end of the AOM/DSS treatment period.

Epimorphin deletion in myofibroblasts alters the morphology and growth of cocultured Caco-2 cells. Epimorphin is abundantly expressed in intestinal myofibroblasts, a major source of epimorphin in the

Figure 3

α-SMA, vimentin, and epimorphin expression in WT and *Epim*^{-/-} colonic myofibroblasts. (A–D) Representative immunofluorescence analyses of WT and *Epim*^{-/-} colon myofibroblasts. Antibody to α-SMA and secondary antibody labeled with Cy3 (A and B), or antibody to vimentin and secondary antibody labeled with fluorescein (C and D), were used. Nuclei were labeled with DAPI (blue). α-SMA and vimentin expression was seen in WT and *Epim*^{-/-} myofibroblasts. Scale bars: 20 μm. (E) Representative immunoblot to quantify epimorphin expression in colonic myofibroblasts obtained from 6 primary cultures from WT (*n* = 3) and *Epim*^{-/-} (*n* = 3) mice. The 34-kDa band corresponds to epimorphin protein. Lower-molecular weight shadow bands represent alternatively spliced syntaxin 2' and 2'' (25). Blots were probed with α-SMA antibody to control for differences in loading.

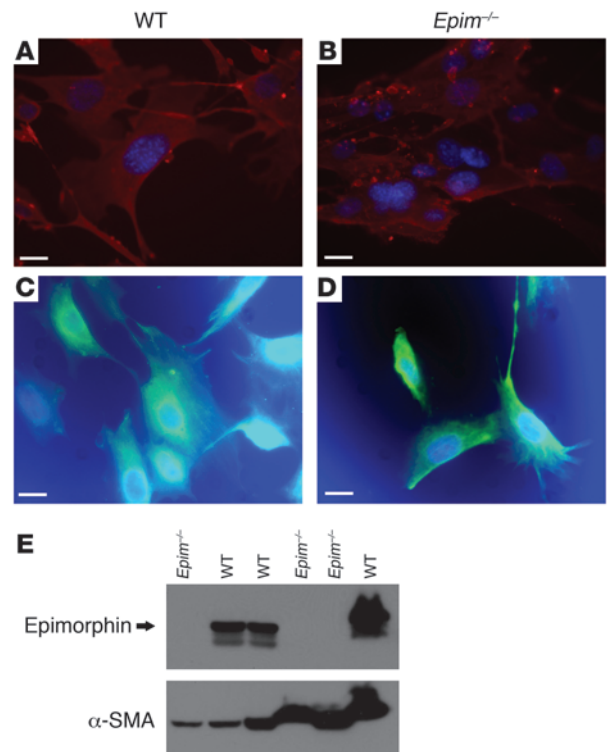
Figure 2

Epimorphin deletion increases colonic crypt cell proliferation in nondysplastic epithelium after AOM/DSS treatment. Mice were treated with AOM/DSS; 90 minutes prior to sacrifice, they were injected with 120 mg/kg 5-BrdU intraperitoneally. Colon sections were incubated with anti-5-BrdU antibody, and antigen antibody complexes were detected with streptavidin-biotin. (A) Labeling index was calculated as the number of 5-BrdU-labeled cells/total number of cells per crypt (WT, *n* = 8; *Epim*^{-/-}, *n* = 6). (B and C) WT (B) and *Epim*^{-/-} (C) descending colon immunostained to detect 5-BrdU. Original magnification, ×100. **P* < 0.05.

gut (19, 23). Immunohistochemical analysis of dysplastic colon revealed that epimorphin was expressed in stroma surrounding areas of dysplasia (Supplemental Figure 4).

To elucidate the mechanisms underlying the protection from epithelial dysplasia in *Epim*^{-/-} mice, primary cultures of colonic myofibroblasts from *Epim*^{-/-} and WT mice were established as described previously (see Methods and ref. 24). Myofibroblast phenotype was confirmed by immunocytochemistry showing robust expression of α-SMA and vimentin (Figure 3, A–D), minimal desmin expression, and absence of expression of epithelial cytokeratin 19 (data not shown), consistent with a colonic myofibroblast phenotype (3) and similar to well-characterized small bowel myofibroblasts (24). Colonic myofibroblasts from WT mice also expressed epimorphin and α-SMA, as determined by immunoblot (Figure 3E). As expected, myofibroblasts from *Epim*^{-/-} mice did not express epimorphin, but produced abundant α-SMA.

To examine the effects of myofibroblasts on the morphology, proliferation, and differentiation of epithelium, we cocultured myofibroblasts with Caco-2 cells (Figure 4). Caco-2 cells have been routinely used in coculture models, as they adhere well to myofibroblasts, exhibit a differentiated enterocyte-like phenotype,



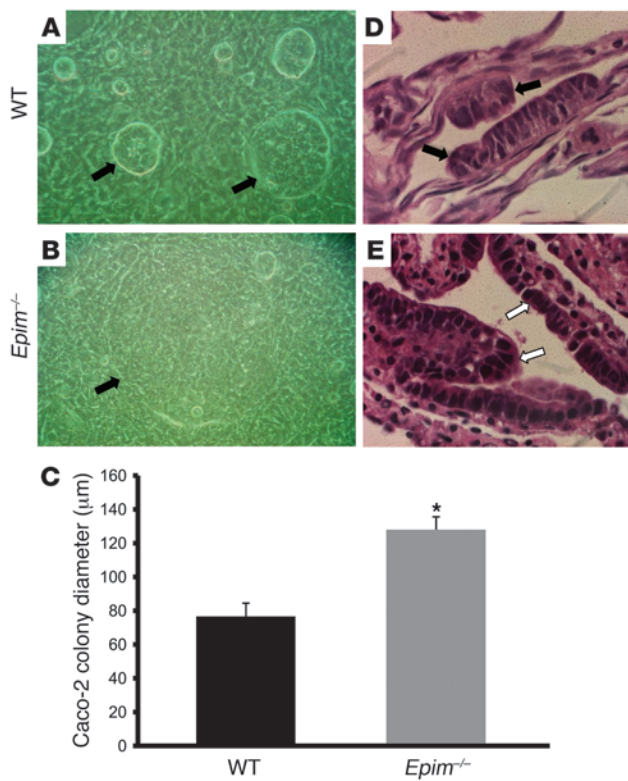


Figure 4

Epimorphin deletion in colonic myfibroblasts alters the morphology of cocultured epithelium. (A and B) Caco-2 cells were seeded on top of WT (A) and *Epim*^{-/-} (B) colon myfibroblasts. Growth and morphology were examined daily with an inverted microscope and photographed on coculture day 4. Caco-2 cells (arrows) cultured on WT myfibroblasts formed small, compact colonies with a central hyperdense area; in contrast, Caco-2 cell colonies cultured on *Epim*^{-/-} myfibroblasts were larger. Original magnification, ×1,000. (C) Mean diameter of Caco-2 colonies grown on *Epim*^{-/-} compared with WT myfibroblasts: *Epim*^{-/-}, 128 μm; WT, 76 μm. (D and E) Histologic analysis of H&E-stained myfibroblast–Caco-2 cocultures. Caco-2 cells cocultured with WT myfibroblasts formed predominantly spherical, compact, multi-layered, pseudostratified epithelial colonies (D, black arrows indicate epithelium). In contrast, Caco-2 cells cocultured with *Epim*^{-/-} myfibroblasts formed an epithelial monolayer (E, white arrows). Original magnification, ×1,000. **P* < 0.05.

and provide reproducible colony morphology (1, 18). Caco-2 cells formed larger colonies on *Epim*^{-/-} colon myfibroblasts compared with Caco-2 colonies grown on WT myfibroblasts, which were small and compact (*Epim*^{-/-}, 128 μm colony diameter; WT, 76 μm colony diameter; *P* < 0.05; Figure 4, A–C). Morphologic analysis showed that Caco-2 cells seeded on WT myfibroblasts formed multiple discrete, spherical, compact, and pseudostratified colonies. In contrast, *Epim*^{-/-} myfibroblasts formed an epithelial monolayer with only occasional small foci of pseudostratified epithelium (Figure 4, D and E). To eliminate the possibility that the morphologic differences were due to differences in adhesion of Caco-2 cells to myfibroblasts, the number of adherent versus floating cells was quantified from media of *Epim*^{-/-} and WT myfibroblast–Caco-2 cocultures. No differences were noted at 24 or 72 hours after plating (data not shown).

Epimorphin deletion alters colonic myfibroblast expression of paracrine factors including components of BMP, Hedgehog (Hh), and Wnt signaling pathways. To further elucidate the molecular basis for the differences in dysplasia in *Epim*^{-/-} compared with WT colon, gene expression profiling of *Epim*^{-/-} versus WT colon myfibroblasts was performed using Agilent microarrays. The total number of genes induced or inhibited greater than 2-fold as a consequence of epimorphin deletion was 2,552 and 3,327, respectively. Because of the large number of genes that exhibited changes in expression, we focused on confirming changes in expression in gene families that encode stromal factors involved in the regulation of colonic epithelial proliferation. These included members of the TGF-β superfamily including the BMP, Hh, and Wnt families (Table 1). Changes in expression were confirmed by quantitative real-time polymerase RT-PCR (qRT-PCR; Supplemental Methods; *n* = 3 independent experiments). Additional key candidate genes

for each signaling pathway were also evaluated by qRT-PCR. Of the TGF-β superfamily members, BMP4 expression was increased 2.1-fold in *Epim*^{-/-} compared with WT myfibroblasts. Marked alterations in expression of BMP inhibitors was noted, including Chordin-1 (68-fold increase), Follistatin (10-fold decrease), and Noggin (64-fold decrease). Gremlin-2 expression was unchanged. Analysis of the Hh signaling pathway showed that expression of Hh family members including Hh-interacting protein (Hhip), Cyclin BI, Patched-2, and Gli-3 were all decreased. In the Wnt family, expression of the Wnt inhibitors Dkk2, Dkk3, and Sfrp4 was increased (2.9- to 6.2-fold); with a 1.5-fold decrease in Sfrp1.

Because the fold change in expression of the BMP inhibitors was widely divergent in *Epim*^{-/-} compared with WT myfibroblasts, we examined the relative expression levels of BMP4 and BMP inhibitors in WT and *Epim*^{-/-} myfibroblasts (Figure 5) to determine which were the most abundantly expressed, and therefore might be the most physiologically relevant. There was abundant BMP4, Chordin-1, Follistatin, and Gremlin-2 mRNA expression in WT and *Epim*^{-/-} myfibroblasts, but significantly lower basal Noggin expression compared with Chordin and BMP4 (*P* < 0.05; Figure 5). The changes in expression were highest for Chordin (68-fold increase) and Noggin (64-fold decrease; *P* < 0.05).

Epimorphin deletion results in increased production and secretion of members of the BMP pathway. BMP4 and Chordin protein expression in cell lysate and media was quantified by ELISA (Supplemental Methods). Chordin expression was significantly increased in *Epim*^{-/-} compared with WT colon myfibroblasts (Figure 6A), and there was a 10-fold increase in Chordin protein secretion from *Epim*^{-/-} versus WT colon myfibroblasts (Figure 6B; *P* < 0.05). In addition, BMP4 protein expression was higher in *Epim*^{-/-} myfibroblasts compared with WT (*P* < 0.05), and BMP4 secretion from unstimulated *Epim*^{-/-} myfibroblasts was 2-fold higher than WT, although the difference was not statistically significant (*Epim*^{-/-}, 79.8 pg/ml; WT, 39.5 pg/ml; *P* = 0.058; Figure 6, C and D).

To determine whether the effect of myfibroblast epimorphin deletion on Caco-2 colony morphology is mediated by Chordin, *Epim*^{-/-} and WT myfibroblasts were cocultured with Caco-2 cells in the presence and absence of Chordin as described previously (25), and Caco-2 colony diameter was measured. Addition of Chordin to WT cocultures increased Caco-2 colony size from 80 to 205 μm (*P* < 0.05; Figure 7). Observation by inverted phase microscopy indicated that addition of Chordin reproduced the phenotype of Caco-2 colonies cocultured with *Epim*^{-/-} myfibro-

**Table 1**

Effects of epimorphin deletion on expression of selected members of the BMP, Hh, and Wnt pathways

Gene	Fold change mRNA <i>Epim</i> ^{-/-} vs. WT
BMP pathway	
Bmp2	1.7
Bmp4	2.1 ^A
Chordin-1	68.3 ^A
Gremlin-2	1.1
Follistatin	-9.7 ^A
Noggin	-64.1 ^A
TGF-β2	2.0 ^A
TGF-β3	1.0
Smad5	1.0
Hh pathway	
Hhip	-100.0 ^A
CyclinB1	-2.6 ^A
Patch-1	-1.2
Patch-2	-1.9 ^A
Gli-1	-1.3
Gli-2	1.4
Gli-3	-1.5 ^A
Wnt pathway	
Fzd3	1.0
Sfrp1	-1.5 ^A
Sfrp4	6.2 ^A
Dkk2	4.4 ^A
Dkk3	2.9 ^A

Fold change in mRNA expression for each gene was determined by qRT-PCR. *n* = 3 independent experiments performed on primary myofibroblast cultures. ^A*P* < 0.05.

blasts, with a predominance of epithelial monolayers in the Chordin-treated cocultures (data not shown). As expected, the size of Caco-2 colonies grown on *Epim*^{-/-} myofibroblasts was unchanged in the presence of additional exogenous Chordin (*P* = NS). These results suggested that increased Chordin secretion was at least partly responsible for the effect of epimorphin deletion on Caco-2 colony morphology.

To correlate these in vitro findings in vivo, we examined the expression of BMP2 and BMP4 as well as the primary end target of BMP signaling, p-Smad1/5/8. Sections of dysplastic colon from WT and *Epim*^{-/-} myofibroblasts were incubated with an anti-BMP2/4 antibody that detects BMP2 expression in colonic epithelial cells (26, 27) and BMP4 expression in stroma (27–29). BMP2 and BMP4 were expressed in WT and *Epim*^{-/-} colon; in a subset of *Epim*^{-/-} colons, a small increase in epithelial and stromal expression was noted (Supplemental Figure 5).

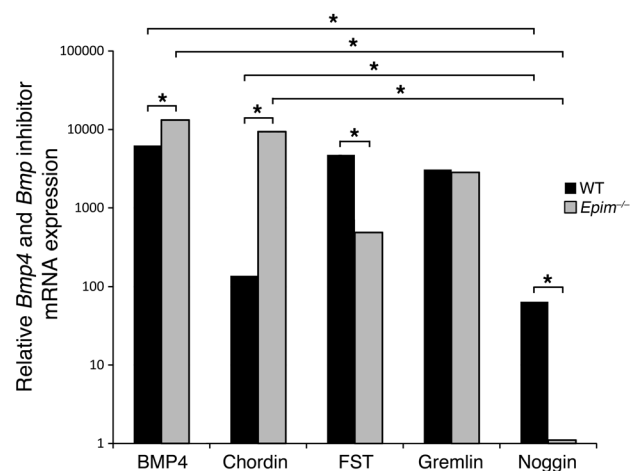
To determine the net effect of epimorphin deletion on BMP signaling in vivo, we examined p-Smad1/5/8 expression by immunohistochemical analysis of AOM/DSS-treated *Epim*^{-/-} and WT colons (Figure 8). There was a marked decrease in p-Smad1/5/8 immunostaining in both normal, nondysplastic *Epim*^{-/-} colon (Figure 8, A and B) and dysplastic descending colon and rectal epithelium (Figure 8, C–F) compared with AOM/DSS-treated WT colon. These findings further suggest that epimorphin deletion in myofibroblasts results in net BMP inhibition.

Epimorphin deletion blunts the colonic myofibroblast response to LPS. Cytokine release plays a key role in tissue damage and the inflam-

matory response in IBD (30). To determine cytokine expression and secretory function in WT and *Epim*^{-/-} myofibroblasts, cells were treated with LPS for 24 hours to mimic the colitis-induced inflammatory milieu. Expression of inflammatory mediators upregulated in acute DSS colitis (TNF-α, IL-6, IFN-γ) with key roles in colitis-associated colon carcinogenesis (31, 32) was evaluated by qRT-PCR. In response to LPS, IL-6 expression increased in WT and *Epim*^{-/-} myofibroblasts compared with unstimulated myofibroblasts (*P* < 0.05; Figure 9A). After exposure to LPS, IL-6 mRNA expression in *Epim*^{-/-} myofibroblasts was decreased compared with WT cells. However, IL-6 protein expression was increased in LPS-stimulated *Epim*^{-/-} myofibroblasts compared with unstimulated *Epim*^{-/-} cells, at levels exceeding those of LPS-stimulated WT cells (Figure 9B). Despite abundant protein expression, *Epim*^{-/-} myofibroblasts did not secrete IL-6 into the media, unlike WT cells (Figure 9C). The profound decrease in IL-6 secretion in response to LPS was not due to absence or downregulation of TLR expression. Myofibroblasts responded to LPS by increasing IL-6 mRNA and protein in both *Epim*^{-/-} and WT myofibroblasts. In addition, TLR4 mRNA was expressed in myofibroblasts, and TLR4 mRNA levels were increased greater than 2-fold in *Epim*^{-/-} compared with WT cells (data not shown).

IFN-γ expression was very low in both *Epim*^{-/-} and WT colon myofibroblasts and was not altered in response to LPS (data not shown). TNF-α mRNA expression in WT and *Epim*^{-/-} myofibroblasts was barely detectable, and was more than 10-fold lower than IL-6 expression. TNF-α protein was not detected in cell lysates, nor was it detectable in secreted form upon LPS stimulation in either WT or *Epim*^{-/-} myofibroblasts (data not shown).

To correlate these in vitro findings in vivo, we performed immunohistochemical analysis of IL-6 expression in AOM/DSS-treated *Epim*^{-/-} and WT colon (Figure 10). IL-6 expression in WT dysplastic colon (Figure 10A) and in normal nondysplastic areas (Figure 10, C and E) was strongest in the stroma, with weak but detectable expression in the epithelium (consistent with previously reported IL-6 expression patterns; ref. 31). In contrast, in dysplastic (Figure 10B) and adjacent nondysplastic colonic

**Figure 5**

Bmp4 and *Bmp* inhibitor mRNA expression in WT and *Epim*^{-/-} myofibroblasts. Relative *Bmp4* and *Bmp* inhibitor mRNA levels were quantified by qRT-PCR as described in Methods. The *y* axis is present in log scale. **P* < 0.05.

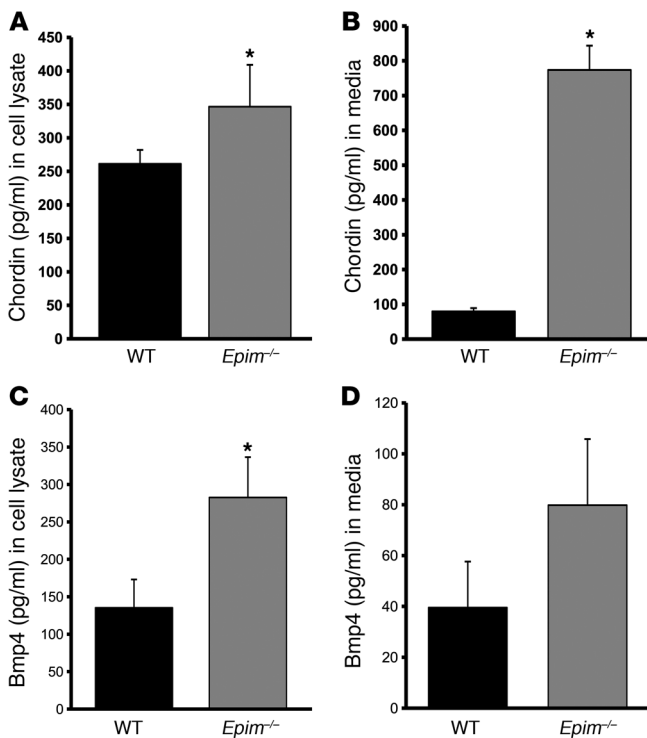


Figure 6

Increased Chordin and BMP4 expression and secretion from *Epim*^{-/-} myofibroblasts. Chordin (A and B) and BMP4 (C and D) expression and secretion were quantified in cell lysates (A and C) and in media (B and D) by ELISA as described in Methods. BMP4 expression in media was higher in *Epim*^{-/-} versus WT myofibroblasts, although the difference was not significant ($P = 0.058$). * $P < 0.05$.

mucosa of AOM/DSS-treated *Epim*^{-/-} mice (Figure 10, D and F), stromal IL-6 expression was markedly diminished compared with WT. Despite the decrease in stromal expression, pericryptal cells at the base of the crypts in *Epim*^{-/-} mice showed expression of IL-6 (Figure 10F), consistent with their ability to synthesize but not secrete IL-6 (Figure 9C).

Serum levels of IL-6 and TNF- α were measured by ELISA in AOM/DSS-treated *Epim*^{-/-} and WT mice, and no significant differences were found (data not shown, $n = 4$ mice per group). Serum concentrations were measured in individual mice, and there was no correlation between tumor burden and serum cytokine levels. These results suggested that epimorphin deletion may not block IL-6 secretion from other cell types, e.g., from myeloid cells such as macrophages (which also express epimorphin; ref. 33) and dendritic cells, the 2 major cellular sources of elevated IL-6 levels in chronic inflammation-associated carcinogenesis (31). To evaluate whether epimorphin deletion inhibits IL-6 secretion from other cell types, we examined the effect of epimorphin deletion on resident peritoneal macrophages, which are reflective of the intestinal environment and well-described in the colitis model (34, 35), and on bone marrow-derived dendritic cells. Resident peritoneal

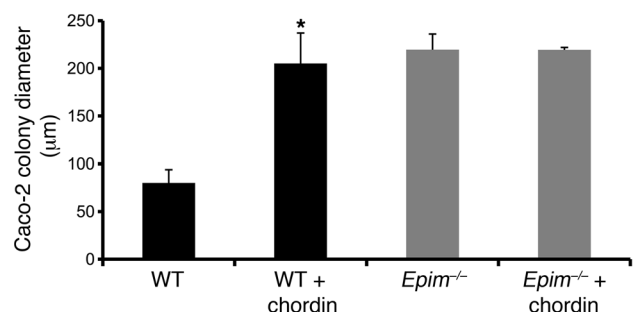
macrophages were cultured as described previously (35, 36), and supernatants were collected for IL-6 assay. Epimorphin deletion significantly diminished, but did not completely block, secretion of IL-6 from resident peritoneal macrophages (689 pg/ml to 272 pg/ml; $P < 0.05$; Supplemental Figure 6). We then evaluated the effect of epimorphin deletion on cultured bone marrow-derived dendritic cells. Because this population does not secrete measurable IL-6 at baseline, cells were treated with LPS for 24 hours, and IL-6 secretion was quantified. Epimorphin deletion did not change IL-6 secretion in response to LPS, which increased in both WT and *Epim*^{-/-} bone marrow-derived dendritic cells (data not shown). These data suggest that epimorphin deletion reduces local IL-6 production from myofibroblasts, and, to a lesser extent, from macrophages, which are uniquely located adjacent to epithelium and the stem cell niche (9).

To rule out the possibility that compensatory changes in other syntaxins resulted in the altered secretory patterns in *Epim*^{-/-} myofibroblasts, we examined expression of syntaxins 1a, 3, and 4, which have the highest percentage homology with epimorphin, and syntaxins 5 and 6, which are also expressed in myofibroblasts (ref. 37 and Supplemental Figure 7). No differences in mRNA expression were noted except for absence of epimorphin, as expected, in *Epim*^{-/-} myofibroblasts.

To further evaluate the altered secretory patterns in *Epim*^{-/-} myofibroblasts, electron microscopy was performed to analyze the ultrastructural morphology of *Epim*^{-/-} and WT myofibroblasts (Figure 11). Parameters included nuclear to cytoplasmic ratios, nuclear membrane regularity and/or roundness, cytoplasmic membrane complexity, length and state of distention of the rough endoplasmic reticulum (RER), and mitochondria. There was an increase in long parallel stacks of RER in *Epim*^{-/-} cells (Figure 11, A and B). In addition, the short stacks of RER were significantly more dilated in *Epim*^{-/-} myofibroblasts (Figure 11C). Dilation of RER is associated with increased accumulation of protein (38, 39), consistent with our findings that synthesis and secretion of IL-6 and a subset of BMP inhibitors were markedly altered by epimorphin deletion. There were no differences in the other morphologic parameters. Because these morphological findings were suggestive of ER stress (40), mRNA expression of the ER stress markers Xbp-1

Figure 7

Chordin alters the morphology of cocultured epithelium. Chordin (2 μ g/ml) was added to WT and *Epim*^{-/-} colon myofibroblast-Caco-2 cocultures. Addition of Chordin to WT myofibroblast-Caco2 cocultures reproduced the morphology of Caco-2 cells cocultured with *Epim*^{-/-} myofibroblasts. The diameter of Caco-2 colonies grown on WT myofibroblasts increased in the presence of Chordin (WT, 80 μ m; WT plus Chordin, 205 μ m) and were similar to the size of Caco-2 colonies grown on *Epim*^{-/-} myofibroblasts. Addition of Chordin did not change Caco-2 colony size on *Epim*^{-/-} myofibroblasts: *Epim*^{-/-}, 219 μ m; *Epim*^{-/-} plus Chordin, 219 μ m. * $P < 0.05$.



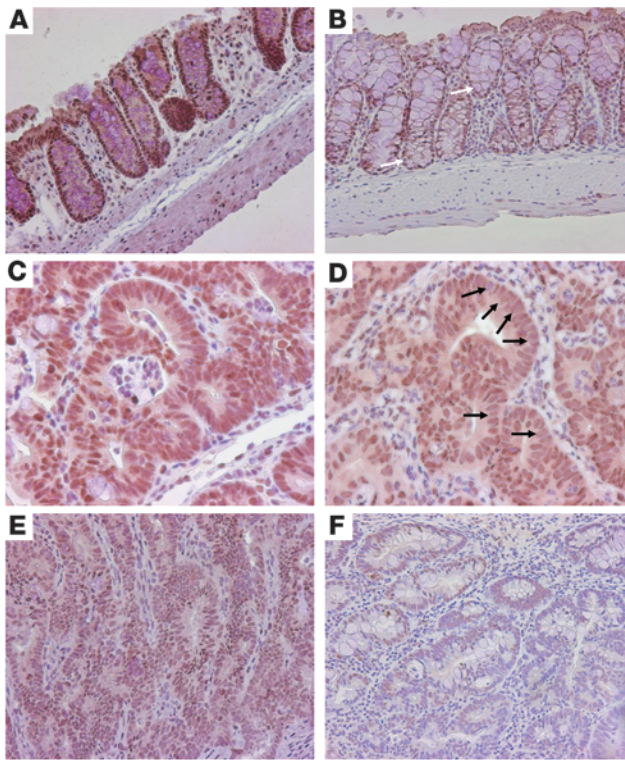


Figure 8 p-Smad1/5/8 expression in *Epim*^{-/-} and WT colon after AOM/DSS treatment. Sections of colon were incubated with polyclonal rabbit anti-p-Smad1/5/8 (1:100 dilution) followed by biotinylated goat anti-rabbit IgG, streptavidin–horseradish peroxidase, and diaminobenzidine. Representative sections of nondysplastic (A and B) and dysplastic colons (C–F) of WT (A, C, E) and *Epim*^{-/-} (B, D, F) mice are shown. (A and B) Decreased or absent brown nuclear staining was noted in *Epim*^{-/-} colon (B, white arrows) compared with homogeneous brown nuclear stain in WT (A). (C and D) p-Smad1/5/8 expression was heterogeneous in *Epim*^{-/-} (D) compared with WT (C) rectal dysplasia, as demonstrated by unstained and less intensely stained nuclei in *Epim*^{-/-} (black arrows). (E and F) Dysplasia from WT descending colon (E) showed light brown nuclear stain, whereas *Epim*^{-/-} dysplastic descending colon (F) showed a marked decrease in nuclear staining compared with WT. Original magnification, $\times 200$ (A, B, E, and F); $\times 400$ (C and D).

unsliced (Xbp-1u), Xbp-1 sliced (Xbp-1s), Atf4, and Grp78 were evaluated. Epimorphin deletion increased Xbp-1u, Xbp-1s, and Atf4 (1.9-, 2.7-, and 1.7-fold, respectively; $P < 0.05$), whereas Grp78 remained unchanged (Figure 11D).

Epimorphin deletion alters Hh signaling. Hh ligands produced by gut epithelial cells act on receptors located on mesenchymal cells to activate downstream stromal target genes (41, 42). Hhip, Gli-1, Gli-2, Gli-3, Patched 1 (Ptc-1), and Ptc-2 are stromal targets of Hh signals, and Hh signaling activity is best reflected by measuring Gli1, Ptc-1, and Hhip mRNA levels (42, 43). Several Hh targets are expressed by both WT and *Epim*^{-/-} colon myofibroblasts, and mRNA levels of a subset of these were decreased in *Epim*^{-/-} compared with WT myofibroblasts (Table 1), including a marked decrease in expression of Hhip, which inhibits Hh signaling and reflects pathway signaling activity. Because Hh ligands are expressed only in epithelial cells, cultured myofibroblasts presumably do not receive Hh signals, and signaling activity is low. To determine the physiologic significance

of the decreased expression of several Hh targets in *Epim*^{-/-} myofibroblasts, myofibroblasts were incubated with recombinant sonic hedgehog (Shh) to determine whether there is also a blunted response to Hh signals. (Ihh and Shh are identical with respect to receptor binding and target gene activation; ref. 44). Expression of Hhip increased 3.5-fold ($P < 0.05$), Gli-1 increased 6.13-fold ($P < 0.05$), and Ptc-1 increased 2.8-fold ($P = 0.07$) in WT myofibroblasts treated with Shh. *Epim*^{-/-} colon myofibroblasts treated with Shh had increased expression of Gli1 only (2.3-fold; $P < 0.01$); however, absolute levels of Gli1 remained 3.7-fold less than in WT ($P < 0.005$). Treatment with Shh did not induce Hhip and Ptc-1 expression in *Epim*^{-/-} myofibroblasts (Figure 12).

Discussion

Deletion of epimorphin reduced the incidence and extent of dysplasia in the AOM/DSS model of inflammation-induced colon carcinogenesis. This protection from dysplasia was associated with increased crypt cell proliferation in adjacent nondysplastic *Epim*^{-/-} epithelium. Epimorphin deletion also affected myofibroblast-epithelial interactions in vitro: WT myofibroblasts cocultured with epithelial Caco-2 cells exhibited small, compact Caco-2 colony morphology with a pseudostratified epithelium; in contrast, Caco-2 cells cocultured with *Epim*^{-/-} myofibroblasts showed increased colony diameter and epithelial monolayer formation. Epimorphin deletion induced marked changes in expression and secretion of a subset of BMP inhibitors, resulting in a net decrease in colonic BMP signaling, as indicated by reduced p-Smad1/5/8 expression. The importance of BMP inhibition was further established by showing that addition of Chordin to WT myofibroblast–Caco-2 epithelial cocultures recapitulated the growth and morphology of Caco-2 colonies cocultured with *Epim*^{-/-} myofibroblasts. Epimorphin deletion also resulted in a profound decrease in LPS-stimulated myofibroblast secretion of the proinflammatory cytokine IL-6, with reduced IL-6 expression in AOM/DSS-treated *Epim*^{-/-} colon. Electron microscopy of *Epim*^{-/-} myofibroblasts depicted morphologic changes in the RER consistent with the marked alteration in synthesis and secretion of IL-6 and Chordin.

Our data suggest that the mechanisms by which epimorphin deletion results in protection from dysplasia are complex, and likely include enhanced epithelial repair resulting from episodic increased crypt cell proliferation as well as reduced epithelial cell damage caused by decreased inflammation. These changes appear to be mediated, at least in part, by inhibition of BMP and IL-6 signaling. In addition, because IL-6 has been postulated to regulate tumor stem cell proliferation, epimorphin deletion may also exert effects on tumorigenesis.

BMP, Wnt, Hh, and Notch signaling interplay in the stem cell niche to regulate intestinal crypt cell proliferation (29, 45–48). Our data showed that expression and secretion of a subset of soluble mesenchymal BMP pathway components were regulated by epimorphin deletion, resulting in decreased BMP signaling in vivo (Figure 8). BMPs and BMP inhibitors originate from the stroma and act on adjacent epithelium (27–29). Expression of these inhibitors is highest toward the base of the crypts, adjacent to the stem cell niche (49). BMPs inhibit crypt cell proliferation, presumably via effects on Wnt– β -catenin signaling mediated by the PTEN–PI3K–Akt pathway (29), although the precise mechanisms are still being clarified (50). A balance between BMPs and BMP inhibitors is thought to play a role in maintaining normal basal levels of crypt cell proliferation (49).

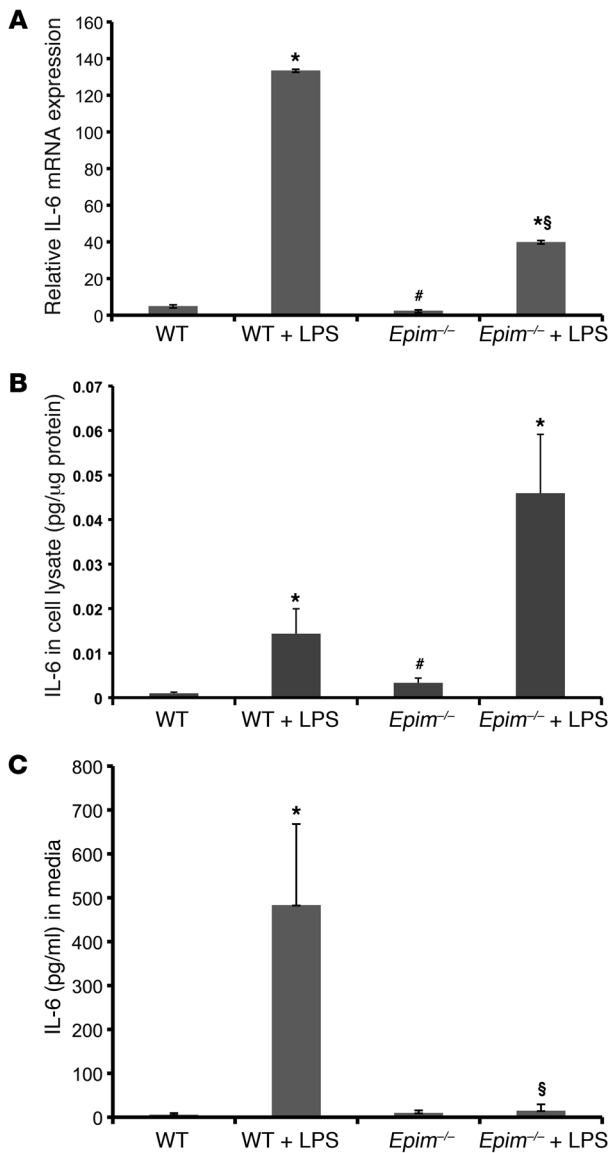


Figure 9

LPS-stimulated IL-6 secretion is altered in *Epim*^{-/-} myofibroblasts. (A) IL-6 mRNA expression in WT and *Epim*^{-/-} myofibroblasts, measured 24 hours after incubation with LPS (5 μg/ml). (B) IL-6 protein expression was stimulated by LPS. IL-6 protein expression in WT and *Epim*^{-/-} myofibroblasts was measured by ELISA after a 24-hour incubation with LPS (5 μg/ml). IL-6 expression was higher in LPS-treated *Epim*^{-/-} myofibroblasts than in LPS-treated WT myofibroblasts, although the difference was not significant ($P = 0.07$). (C) IL-6 protein secretion was markedly reduced in LPS-treated *Epim*^{-/-} myofibroblasts. Cells were incubated with LPS (5 μg/ml) for 24 hours. * $P < 0.05$ versus respective untreated group; # $P < 0.05$ versus untreated WT; § $P < 0.05$ versus LPS-treated WT.

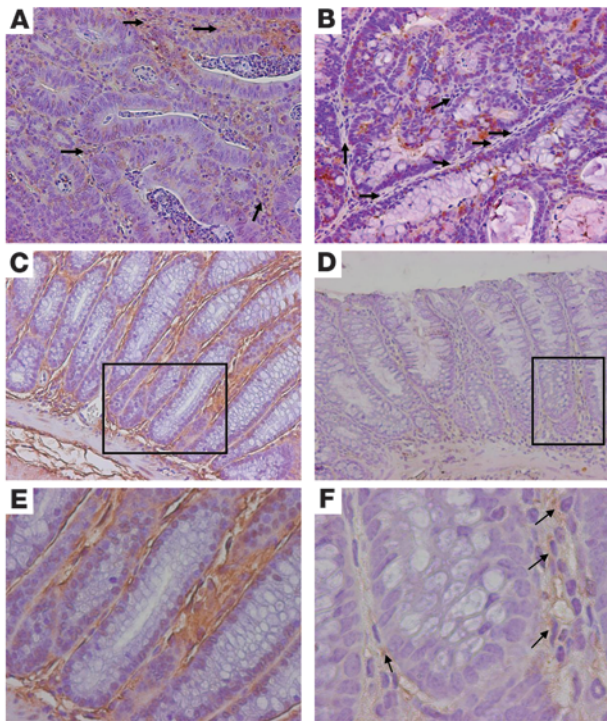
and markedly enhanced epithelial proliferation rate. Although BMP inhibition is likely to result in unopposed Wnt signaling, epimorphin deletion resulted in decreased dysplasia. We postulate that in our model, BMP inhibition results in enhanced epithelial repair and that this, in conjunction with markedly reduced IL-6 secretion, leads to partial protection from dysplasia.

Epimorphin deletion completely blocked IL-6 secretion by myofibroblasts, and in vivo analysis of IL-6 expression in *Epim*^{-/-} and WT dysplasia in the AOM/DSS model demonstrates that epimorphin deletion results in diminished stromal IL-6 expression. We also showed that epimorphin deletion reduced IL-6 secretion by peritoneal macrophages, but not by bone marrow-derived dendritic cells. Reduced stromal IL-6 likely results in decreased epithelial cell damage (38). In addition, IL-6 is active in the tumor stem cell niche (52); reduced secretion may also result in decreased proliferation of dysplastic premalignant cells, thus suggesting a direct effect on tumorigenesis (31, 52). Our data are consistent with studies from other laboratories (31, 32, 53) that have shown that IL-6 plays a key role in the pathogenesis of colitis-associated carcinogenesis. The pleiomorphic effects of epimorphin deletion on secretion of multiple factors, particularly IL-6, likely explains why the observed increase in colonic crypt cell proliferation did not result in larger tumors, as in other genetic models of chronic inflammation-associated carcinogenesis, such as the SOCS3-null mouse (32). It is likely that the end result of epimorphin deletion is a change in secretion of soluble factors that overall has beneficial effects, resulting in reduced dysplasia.

Wnt signaling is critically important in regulating normal crypt cell proliferation and is dysregulated in colon carcinogenesis. In colitis-associated neoplasia, *Apc* mutations are much less common compared with sporadic colon cancer and occur later in the disease (20, 54). Both epithelial and mesenchymal cells express Wnts (55), but the precise sources and regulation of Wnt secretion are still being clarified. Expression of several Wnt inhibitors was upregulated in *Epim*^{-/-} myofibroblasts. However, epimorphin deletion did not alter expression of nuclear β-catenin or cyclin D1 in dysplastic tumors and did not affect the proportion of low- and high-grade dysplastic lesions. The significance of the change in expression of Wnt inhibitors is unclear from our studies, which evaluated Wnt target gene expression at an advanced stage of the disease process. Following *Apc* mutation, nuclear β-catenin signaling becomes dysregulated, and changes in Wnt ligand expression may no longer affect downstream signaling; however, it is possible that enhanced secretion of Wnt inhibitors earlier in the disease course, prior to *Apc* mutation, may diminish proliferation of dysplastic epithelium.

The net effect of epimorphin deletion is inhibition of BMP signaling in the epithelium, as indicated by decreased p-Smad1/5/8 expression (Figure 8). This would be expected to lead to an increase in crypt cell proliferation, as shown in Figure 2. Although expression of a subset of BMP inhibitors is decreased in *Epim*^{-/-} myofibroblasts (Figure 5), and BMP4 expression and secretion were increased (Figures 5 and 6), it is likely that Chordin's inhibitory actions are locally dominant in the crypt due to its 10-fold increased secretion. Chordin's key role is further supported by its effects in *Epim*^{-/-} myofibroblast cocultures (Figure 7). We postulate that in *Epim*^{-/-} mice, BMP inhibition stimulates enhanced crypt cell proliferation early in the course of AOM/DSS-induced disease, resulting in enhanced epithelial repair and decreased tumorigenesis.

Our model appears to result in partial, but not complete, BMP inhibition, as indicated by persistent, albeit reduced, p-Smad1/5/8 expression. Complete BMP inhibition might be expected to result in a tumorigenic phenotype, as in mice that have a nonfunctional BMP receptor BMPRI1A (51), or in Noggin-overexpressing mice (27, 28), both of which result in a juvenile polyposis phenotype

**Figure 10**

IL-6 expression in *Epim*^{-/-} and WT colon after treatment with AOM/DSS. Sections of colon were incubated with goat anti-IL-6 antibody (1:50 dilution). Representative sections of dysplastic (A and B) and nondysplastic (C–F) WT (A, C, E) and *Epim*^{-/-} (B, D, F) colons are shown. (A) WT dysplastic colon showed light brown stromal staining (arrows), and scattered epithelial cells were positive for IL-6. (B) Dysplastic *Epim*^{-/-} colon exhibited less stromal staining (arrows), and scattered brown epithelial cells were seen. (C and D) Nondysplastic *Epim*^{-/-} colon (D) demonstrated less stromal IL-6 than did WT (C). (E and F) Higher-magnification views of boxed regions in C and D, showing intense cellular and extracellular stromal staining in nondysplastic WT colon (E) and markedly reduced staining in *Epim*^{-/-} colon (F). Scattered pericryptal cells in *Epim*^{-/-} colon showed persistently positive staining (arrows). Original magnification, ×200 (A–D); ×400 (E); ×1,000 (F).

We have shown that the function of *Epim*^{-/-} myofibroblasts was profoundly altered, resulting in marked changes in myofibroblast secretory function. These effects are likely due to epimorphin's role as a syntaxin. These membrane-bound proteins have an intracellular, cytoplasmic orientation and are involved in trafficking of secretory vesicles. Our data suggest epimorphin deletion results in marked and specific alteration in secretory function, indicating that particular syntaxins may regulate the release of a subset of secreted proteins. Altered secretory function was not caused by compensatory changes in expression of other syntaxins in *Epim*^{-/-} myofibroblasts (Supplemental Figure 7) or in *Epim*^{-/-} intestine (19). IL-6 secretion from WT myofibroblasts was stimulated in response to LPS, but completely blocked in *Epim*^{-/-} myofibroblasts. This occurred despite an increase in IL-6 mRNA and protein production in both *Epim*^{-/-} and WT cells, suggesting a profound alteration in the IL-6 secretory process. In contrast, Chordin and BMP4 secretion were increased. The consequences of epimorphin deletion may be pathway dependent, and appear to differ in stimulated versus constitutive secretory processes. In the mammary gland, epimorphin is itself secreted (12, 17). However, immunoblot of concentrated media from WT myofibroblasts showed virtually no secretion of epimorphin, despite abundant cellular protein expression (data not shown).

Epim^{-/-} myofibroblasts showed decreased expression of Hh target genes after exposure to Hh ligands compared with WT myofibroblasts. These data suggest that deletion of epimorphin also affects the myofibroblast's ability to respond to soluble factors that signal to the mesenchyme. Unlike in other epithelial cancers, in which activated Hh signaling results in increased proliferation, active Hh signaling has been shown to inhibit crypt cell proliferation in the colon and small bowel (46). It is possible that this change in responsiveness to Hh signals contributes to enhanced crypt cell proliferation in the *Epim*^{-/-} mice, but further studies are required to interrogate this complex pathway.

Overall, our data suggest that protection from dysplasia is likely mediated, at least in part, by changes in the function and secretory profile of intestinal subepithelial myofibroblasts. Our results suggest potentially novel pathogenetic mechanisms of inflammation-induced colonic dysplasia, which may be relevant for patients with IBD. Our data suggest that the stromal environment, including the myofibroblast, plays a significant role in inflammation-induced dysplasia. Although stromal interactions with the epithelium have been suggested to play a pathogenic role in colorectal carcinogenesis and inflammation-induced colon cancer, the epimorphin deletion mouse model is unique because myofibroblast secretory function has been altered. MSCs have been increasingly recognized to play an important role in wound repair in epithelial tissues (7, 8, 56). Whether the MSC or a more differentiated progeny cell is responsible for cross-talk within the stem cell niche is unclear. Our studies suggest that the myofibroblast may be one of the MSC progeny that is active within the stem cell niche. These studies also suggest what we believe to be a novel therapeutic target for treatment of IBD and prevention of colorectal cancer, since modifying myofibroblast function appears to affect epithelial cell proliferation and the incidence and severity of dysplasia.

In summary, epimorphin deletion showed beneficial effects in 2 colitis/injury models, the acute DSS-induced colitis model (19) and the AOM/DSS model of colitis-associated carcinogenesis, which suggests that modulating the function of this myofibroblast protein may have a therapeutic effect in the appropriate clinical setting. Our results confirm the complexity of mesenchymal-epithelial interactions and suggest a role for myofibroblasts in colonic injury, repair, and carcinogenesis. We have shown that, in the AOM/DSS model, an intervention resulting in increased crypt cell proliferation may still have beneficial effects even in the long term. Thus, therapies that increase epithelial repair and crypt cell proliferation while reducing inflammatory damage may have a place in the IBD/

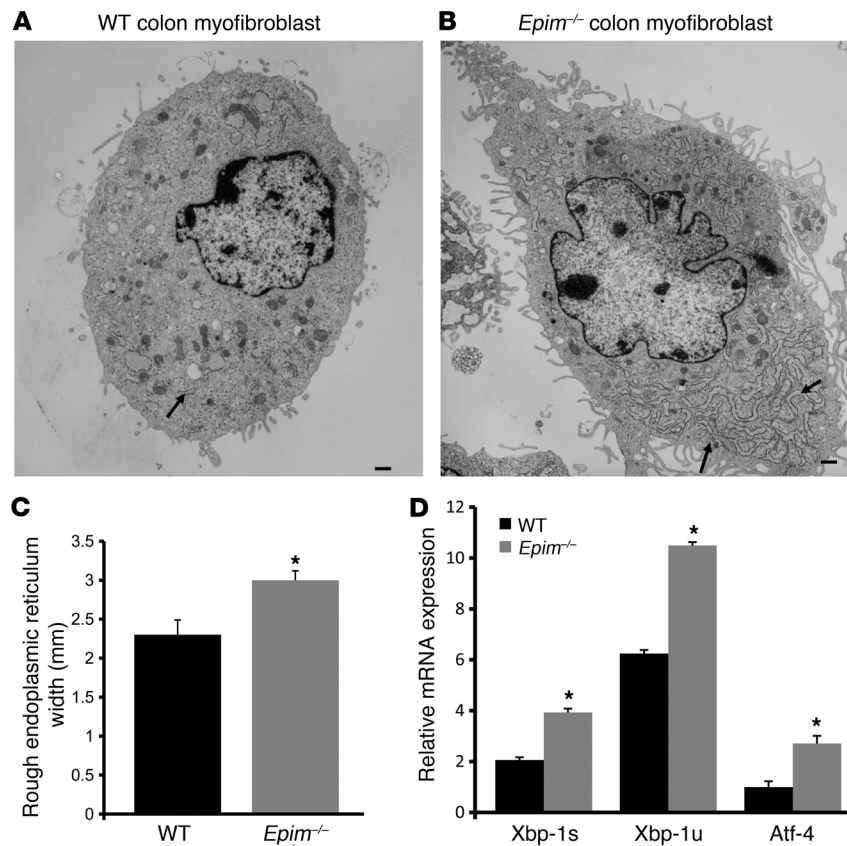


Figure 11

Electron microscopic analysis of *Epim*^{-/-} and WT myofibroblasts. (A) WT colon myofibroblast. (B) *Epim*^{-/-} colon myofibroblast. Note the increase in RER stacks (arrows) in *Epim*^{-/-} myofibroblasts compared with those in WT myofibroblasts. Scale bars: 1 μm. (C) Quantification of RER dilation. The shorts stacks of RER were more dilated in *Epim*^{-/-} myofibroblasts than in WT myofibroblasts. (D) Increased expression of ER stress markers in *Epim*^{-/-} myofibroblasts. *Xbp-1s*, *Xbp-1u*, and *Atf-4* mRNA levels were quantified by qRT-PCR (*n* = 3 independent experiments). **P* < 0.05.

chronic inflammatory disorder armamentarium. Since epimorphin is widely expressed in the stroma of other epithelial tissues, these data may have relevance to other inflammation-induced epithelial cancers, such as those in pancreas, esophagus, and skin.

Methods

Animals. *Epim*^{-/-} mice, with a global deletion of epimorphin, were generated as described previously (19), and C57BL/6J WT littermates or C57BL/6J mice purchased from Jackson Laboratory were used as controls. Mice purchased from Jackson Laboratory were acclimated to the animal facility for 3.5 weeks. Mice were housed in a 12-hour light/dark cycle with free access to food and water. Mice were fed a standard rodent chow diet (PicoLab 20; Purina). Age-matched 8- to 12-week-old *Epim*^{-/-} mice and their WT littermates were used in all experiments. All animal experimentation was approved by the Animal Studies Committee of Washington University School of Medicine.

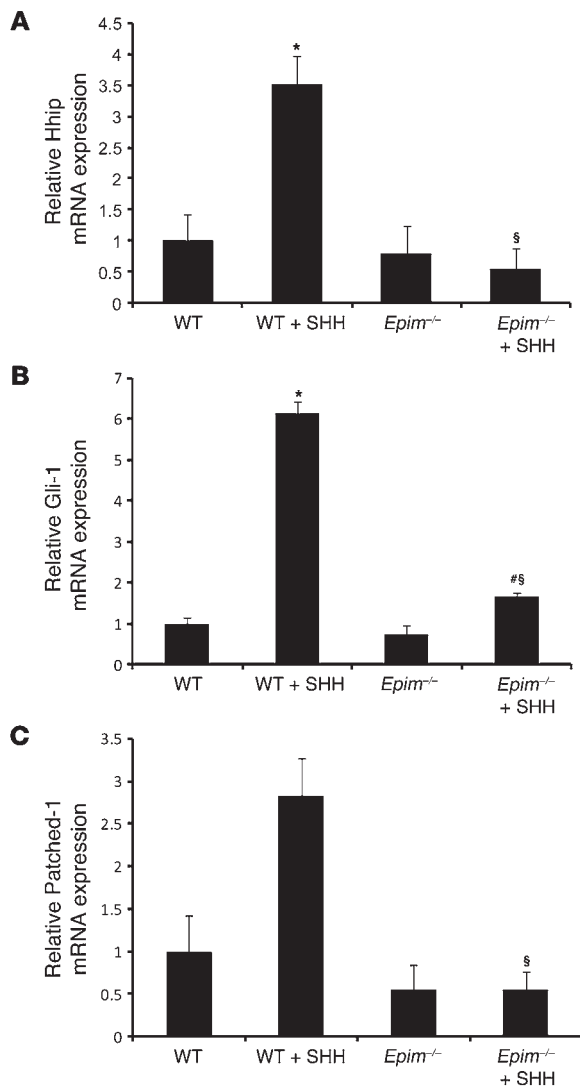
AOM/DSS model for colitis-induced carcinogenesis. Congenic *Epim*^{-/-} mice (on a C57BL/6J background; *n* = 17) and WT C57BL/6J mice (*n* = 22) were injected with AOM (13.5 mg/kg; Sigma-Aldrich) on day 0 (Supplemental Figure 1). On day 5, 3 cycles of DSS (2.5%, 3%, 3% in drinking water; 5 days/cycle) were initiated, each separated by 15 days of vehicle control (water). This regimen was chosen based on pilot studies showing that a previously published lower-dose regimen (21, 22) of AOM (12.5 mg/kg) followed by 3 cycles of 2.5%, 2.5%, 2% DSS in drinking water did not result in dysplasia in our mice. Mice were sacrificed 20 days after completion of the third DSS cycle, and tissues were placed into 10% formalin for histology. The presence and grade of dysplasia (low versus high grade) was evaluated as described previously (57). Apoptosis was evaluated by routine histologic methods on H&E-stained tissue (58). Serum was collected, and ELISA was performed

per the manufacturers' instructions for TNF-α, IFN-γ (BD Biosciences), and IL-6 (eBioscience).

Crypt cell proliferation. At 90 minutes prior to sacrifice, mice were injected intraperitoneally with 5-BrdU (8 g/l) and 5-fluorodeoxyuridine (0.8 g/l), total dose 120 mg/kg. 5-BrdU was detected with a monoclonal anti-BrdU antibody (Zymed Laboratories Inc.), and crypt cell proliferation was assessed as described previously (19). To correct for differences in crypt depth, labeling index was calculated as the number of 5-BrdU-positive cells per total crypt cell number (19). Crypt cell proliferation indices were also quantified separately in areas adjacent to ulcerations and were compared in WT and *Epim*^{-/-} mice.

Quantification of polyposis and dysplasia. Grossly visible polyps were counted and diameters measured. Tumor area and total colon area were measured using Metaview software, and the percentage of tumor area per total colon area was calculated. Colons were divided into cecum, proximal, and distal colon, sectioned, and stained with H&E. The entire colon was analyzed for dysplasia by light microscopy (magnification, ×40; the presence of dysplasia was confirmed under higher-power magnification, ×100). The number of fields of vision was counted, and the percentage with dysplasia was calculated as the number of dysplastic segments per fields of vision. The diameter of dysplastic lesions was measured with Axiovision software (Zeiss).

Generation of *Epim*^{-/-} and WT colon myofibroblast primary cultures. 3 *Epim*^{-/-} and 3 WT colon myofibroblast primary cultures were established as previously described (24, 59) from WT and *Epim*^{-/-} 7- to 9-day-old mice. Briefly, colon from cecum to rectum was placed in HBSS (Invitrogen), washed briefly, transferred into fresh HBSS, and minced into 2- to 3-mm pieces. Tissue was washed 8 times with HBSS by vigorous shaking, allowing for fragments of colon to sediment out; incubated with 300 U/ml collagenase XI (Sigma-Aldrich) and 0.1 mg/ml dispase (Gibco, Invitrogen) for 25 minutes at room temperature

**Figure 12**

Epimorphin deletion alters hedgehog signaling. WT and *Epim*^{-/-} colon myofibroblasts were incubated with recombinant Shh (0.9 μ g/ml) for 24 hours, and mRNA levels of Hh end targets *Hhip*, *Gli-1*, and *Patched-1* were quantified by qRT-PCR. WT myofibroblasts responded to Shh with an increase in *Hhip* (A), *Gli-1* (B), and *Patched-1* (C) mRNA (the difference in *Patched-1* levels between treated and untreated WT was not significant; $P = 0.07$). Unlike *Gli-1* mRNA, *Hhip* and *Patched-1* expression did not increase in *Epim*^{-/-} myofibroblasts in response to Shh, and expression of all 3 end targets in Shh-treated *Epim*^{-/-} myofibroblasts was less than that in Shh-treated WT myofibroblasts. * $P \leq 0.05$ versus WT; # $P < 0.05$ versus untreated *Epim*^{-/-}; § $P < 0.05$ versus Shh-treated WT.

myofibroblasts between passages 6–9, cultured for 1 week. Total RNA from which probes were generated was prepared from a pool of 3 myofibroblast isolates for each. Probes were hybridized to Agilent microarrays as per the Genomics Core of the Digestive Diseases Research Core Center (DDRCC, Washington University School of Medicine). The data set was searched to identify putative epimorphin targets that exhibited greater than 2-fold increase or less than 0.5-fold decrease in expression between *Epim*^{-/-} and WT colon myofibroblasts (GenePix 6.0 acquisition and analysis software; ref. 18), focusing on members of the BMP/TGF- β , Wnt, and Hh families. Changes in expression of selected genes on microarray were all confirmed by qRT-PCR.

Immunocytochemistry. Primary cultures of colonic myofibroblasts and Caco-2 cell lines were grown on chamber slides (Nalge Nunc International) and fixed in 10% formalin (room temperature) for 10 minutes, permeabilized with ice-cold methanol, and stored at -20°C . After incubation in blocking solution containing 5% BSA and 3% milk in Tris buffer (20 mM Tris HCl; 150 mM NaCl, pH 7.4; and 0.05% Tween 30) for 60 minutes, slides were incubated with primary antibody diluted in blocking solution at 4°C overnight. To confirm the myofibroblast phenotype, rabbit polyclonal antibodies to α -SMA (ab5694, 1:200 dilution; Abcam); desmin (D8281, 1:100 dilution; Sigma-Aldrich); cytokeratin 18 (1:100 dilution; Millipore Corp.); vimentin (V4630, 1:100 dilution; Sigma-Aldrich); were used. Secondary antibody labeled with fluorescein or Cy3 diluted in blocking solution was applied for 1 hour at room temperature. Cells were mounted in Vectashield Mounting Medium with DAPI and examined under a fluorescence microscope (Axioshop 2; Carl Zeiss Jena GmbH).

Immunohistochemical analyses. Epimorphin expression in WT colon was analyzed as described previously (19) using a polyclonal rabbit anti-syntaxin 2 antibody (1:500 dilution; Synaptic Systems) that was purified to remove cross-reactivity with other syntaxins, by preabsorption with total protein isolated from *Epim*^{-/-} mouse intestine (1 μ g antibody incubated with 50 μ g protein). Epitope retrieval was with the Nuclear DECLOAKER reagent (BIOCARE) in a decloaking chamber. Primary antibody was applied overnight at 4°C . Antigen antibody complexes were detected with biotinylated goat anti-rabbit IgG (1:2,000 dilution) and donkey anti-goat IgG (1:2,000 dilution; Jackson ImmunoResearch Laboratories Inc.) and streptavidin–horseradish peroxidase with tyramide amplification, then developed in diaminobenzidine.

BMP2/BMP4 expression was detected as described previously (19) using a polyclonal goat anti-human BMP2/4 antibody (1:300 dilution; R&D Systems) that cross-reacts with mouse, and antigen retrieval with citraconic anhydride. p-Smad1/5/8, nuclear β -catenin, and cyclin D1 expression was detected using a polyclonal rabbit anti-p-Smad1/5/8 (1:100 dilution; Millipore), polyclonal rabbit anti- β -catenin antibody (1:600 dilution; BD Transduction Laboratories), and rabbit anti-cyclin D1 antibodies (1:200; Santa Cruz). Antigen retrieval for p-Smad1/5/8, nuclear β -catenin, and cyclin D1

with gentle shaking; and then centrifuged at low speed (4 g) for 10 minutes. Supernatant was discarded. The pellet, containing intact organoids with attached myofibroblasts, was transferred to a 1.7-ml tube, minced with scissors, and washed 5 times in DMEM (Gibco, Invitrogen) with 2% sorbitol (Sigma-Aldrich) to eliminate isolated cells and then centrifuged 1–2 minutes at low speed. Cells were seeded in 6-well plates and cultured in DMEM with 10% FBS (US Biotechnologies Inc.), insulin (Sigma-Aldrich), transferrin (Roche), and gentamicin (Calbiochem EMD Chemicals), all 10 μ g/ml, as well as 2 ng/ml EGF (Sigma-Aldrich). After 4 days, mesenchyme-derived cells were passaged to T25 flasks using 0.05% trypsin in 0.53 mM EDTA (Cellgro, Mediatech). Under these conditions, epithelial cells do not survive.

Caco-2 cell culture. The Caco-2 human colon cancer epithelial cell line was grown as described previously (18). Cell lines were passaged every 4–7 days.

RNA analysis by qRT-PCR. qRT-PCR was performed as described previously (19); see Supplemental Methods for details. SuperScript II Reverse Transcriptase (Invitrogen) was used for synthesis of cDNA. Real-time RT-PCR analysis using SYBR green PCR Master Mix (Applied Biosystems) was performed in an ABI Prism 7700 sequence detection system (Applied Biosystems). Primer sequences are listed in Supplemental Table 1.

Gene expression profiling. To determine the identity of putative myofibroblast morphogens, total RNA was prepared from *Epim*^{-/-} and WT colon



was performed with Diva Decloaker reagent (BIOCARE). Antigen-antibody complexes were detected with biotinylated goat anti-rabbit IgG (1:500 dilution; PerkinElmer), streptavidin-horseradish peroxidase, and diaminobenzidine. IL-6 expression was detected using a goat anti-recombinant mouse IL-6 antibody (1:50 dilution; R&D systems) followed by a biotinylated donkey anti-goat antibody (1:500 dilution; Jackson ImmunoResearch Laboratories), streptavidin-horseradish peroxidase, and diaminobenzidine.

LPS stimulation of myofibroblasts. *Epim*^{-/-} and WT colon myofibroblasts were seeded at a density of 2×10^5 cells per well in 6-well plates and grown to 85% confluence. Cultured myofibroblasts were incubated with LPS (2.5, 5, and 10 $\mu\text{g/ml}$ in serum-free media) for 6 hours (List Biological Laboratories Inc.). Based on this dose response, cells were incubated for 24 hours with LPS (5 $\mu\text{g/ml}$). Supernatant was collected for ELISA. Cells were harvested for RNA and protein for qRT-PCR and ELISA as described above and in Supplemental Methods. qRT-PCR data was expressed as fold induction relative to untreated samples.

Resident peritoneal macrophage isolation. Resident peritoneal macrophages were isolated by flushing the peritoneal cavity with cold PBS as described previously (35, 36, 60). Cells were counted for viability by trypan blue exclusion; plated (5×10^5 cells/well) in a 96-well plate in RPMI 1640 media (BioWhittaker) with 2 mM L-glutamine (Life Technologies), 10 mM HEPES, 1 mM sodium pyruvate (BioWhittaker), 50 U/ml penicillin and 50 mg/ml streptomycin (Life Technologies), 50 mM 2-ME (Fisher Scientific), and 10% FCS (HyClone); and cultured at 37°C in 5% CO₂. After 24 hours, supernatants were collected for determination of IL-6 secretion by ELISA (Supplemental Methods).

Generation of bone marrow-derived dendritic cells. Dendritic cells were generated from mouse bone marrow progenitors as described previously (61). Bone marrow cells were harvested from femurs of *Epim*^{-/-} and WT mice ($n = 2$) and cultured in 6-well plates with GM-CSF (10 ng/ml) and IL-4 (0.3 ng/ml) in RPMI 1640 media supplemented as described above. Media containing GM-CSF and IL-4 was replaced on days 3 and 6 of culture. On day 7, cells were harvested; a portion was evaluated by flow cytometry to confirm the generation of dendritic cells. Remaining dendritic cells were plated in 96-well plates (5×10^5 cells/well) and treated with LPS (1 mg/ml) for 24 hours. Cells were harvested for RNA isolation, and supernatant was collected for evaluation of IL-6 secretion by ELISA.

SHH signaling in myofibroblasts. *Epim*^{-/-} and WT colon myofibroblasts were seeded at a density of 2×10^5 cells/well in 6-well plates and grown to 85% confluence. Cells were incubated with recombinant mouse SHH aminoterminal peptide (0.9 $\mu\text{g/ml}$; R&D Systems) diluted in serum-free media; after 24 hours, cells were harvested, and RNA was isolated for qRT-PCR.

Myofibroblast-Caco-2 coculture experiments. *Epim*^{-/-} and WT colon myofibroblasts were plated as previously described (ref. 18; 1×10^6 cells/well) and cultured for 3 days in 6-well plates (Costar Corning Inc). Caco-2 cells were seeded on top of subconfluent layers of myofibroblast cells (3×10^5 cells/well). To assess adherence of the Caco-2 cells to the *Epim*^{-/-} and WT myofibroblasts, media was collected at 24 and 72 hours after plating, and cells were counted; no differences in cell adherence were found ($n = 2$ experiments). Cocultures were examined daily by inverted phase microscopy, and photomicrographs were taken on day 4 after plating. To quantify dif-

ferences in Caco-2 colony size and assess morphology, photomicrographs were taken from 4 quadrants per well. The diameter of each Caco-2 colony was measured using Axiovision software (Zeiss). After 7 days, cocultures were fixed in paraformaldehyde and processed for histology.

Chordin (2 $\mu\text{g/ml}$; R&D Systems) was added to media immediately after Caco-2 cells were seeded and again on day 3 of coculture. Morphology and colony diameters were measured on day 4 as described above.

Electron microscopic analysis. *Epim*^{-/-} and WT colon myofibroblasts were grown to confluence in T25 flasks ($n = 2$ independent experiments), harvested with trypsin/EDTA, fixed with 2.5% glutaraldehyde, and processed for electron microscopy by the Electron Microscopy Core, Washington University School of Medicine. A total of 20 *Epim*^{-/-} cells and 15 WT cells were observed at $\times 3,000$ and $\times 4,400$ magnification, and images were obtained from several quadrants of each section. Nuclear/cytoplasmic ratio, nuclear membrane regularity and roundness, cytoplasmic membrane complexity, length of the rough ER, and mitochondria were evaluated in a semiquantitative manner, using magnification prints and a transparent 0.2-cm grid. A total of 48 prints were scored. The state of dilation of the short stacks of rough ER was assessed for 16 *Epim*^{-/-} and 11 WT cells. Each cell was divided into 4 quadrants. The width of 3–5 stacks of rough ER in each quadrant was measured using the transparent grid, and the average width of rough ER was calculated for each quadrant. Images were independently reviewed by a pathologist blinded to the genotype.

Statistics. Data comparing *Epim*^{-/-} and WT mice are presented as mean \pm SEM, and significance was analyzed by 2-tailed Student's *t* test (Microsoft Excel; Microsoft). *P* values less than or equal to 0.05 were considered significant. Mortality rates were compared in *Epim*^{-/-} and WT mice using the Fisher exact probability test (Vassarstats).

Acknowledgments

We thank Kymberli Carter for help with immunostaining; Marilyn Levy (Electron Microscopy Core, Department of Cell Biology, Washington University School of Medicine), Valerie Blanc, and Keely McDonald for advice and technical assistance; and Nicholas Davidson for advice and manuscript review. These studies were supported by NIH National Institute of Diabetes and Digestive and Kidney Diseases (NIDDK) grants DK61216, DK46122 (D.C. Rubin), and DK50466 (M.S. Levin); by an American Gastroenterological Association Fellowship to Faculty Transition Award and a DDRCC Pilot and Feasibility award (A. Shaker); and by NIH NIDDK grant DK52574 (Morphology and Mouse Models Cores, DDRCC, Washington University School of Medicine).

Received for publication August 3, 2009, and accepted in revised form March 3, 2010.

Address correspondence to: Deborah C. Rubin, Division of Gastroenterology, Washington University School of Medicine, 660 South Euclid Avenue, Box 8124, St. Louis, Missouri 63110, USA. Phone: 314.362.8935; Fax: 314.362.8959; E-mail: drubin@wustl.edu.

- Kedinger M, Duluc I, Fritsch C, Lorentz O, Plateroti M, Freund JN. Intestinal epithelial-mesenchymal cell interactions. *Ann N Y Acad Sci.* 1998;859:1–17.
- Coussens LM, Werb Z. Inflammation and cancer. *Nature.* 2002;420(6917):860–867.
- Powell DW, Mifflin RC, Valentich JD, Crowe SE, Saada JI, West AB. Myofibroblasts. II. Intestinal subepithelial myofibroblasts. *Am J Physiol.* 1999;277(2 pt 1):C183–C201.
- Hayward SW. Approaches to modeling stromal-epithelial interactions. *J Urol.* 2002;168(3):1165–1172.
- Kedinger M, Simon-Assmann PM, Lacroix B, Marxer A, Hauri HP, Haffen K. Fetal gut mesenchyme induces differentiation of cultured intestinal endodermal and crypt cells. *Dev Biol.* 1986;113(2):474–483.
- Duluc I, Lorentz O, Fritsch C, Leberquier C, Kedinger M, Freund JN. Changing intestinal connective tissue interactions alters homeobox gene expression in epithelial cells. *J Cell Sci.* 1997;110 (pt 11):1317–1324.
- Stappenbeck TS, Miyoshi H. The role of stromal stem cells in tissue regeneration and wound repair. *Science.* 2009;324(5935):1666–1669.
- Andoh A, Bamba S, Brittan M, Fujiiyama Y, Wright NA. Role of intestinal subepithelial myofibroblasts in inflammation and regenerative response in the gut. *Pharmacol Ther.* 2007;114(1):94–106.
- Andoh A, Bamba S, Fujiiyama Y, Brittan M, Wright NA. Colonic subepithelial myofibroblasts in mucosal inflammation and repair: contribution of bone marrow-derived stem cells to the gut regenerative response. *J Gastroenterol.* 2005;40(12):1089–1099.
- Powell DW. Myofibroblasts: paracrine cells important in health and disease. *Trans Am Clin Climatol Assoc.* 2000;111:271–292; discussion 292–293.
- Hirai Y, Lochter A, Galosy S, Koshida S, Niwa S, Bissell MJ. Epimorphin functions as a key morpho-



- regulator for mammary epithelial cells. *J Cell Biol.* 1998;140(1):159–169.
12. Radisky DC, Hirai Y, Bissell MJ. Delivering the message: epimorphin and mammary epithelial morphogenesis. *Trends Cell Biol.* 2003;13(8):426–434.
13. Bennett MK, et al. The syntaxin family of vesicular transport receptors. *Cell.* 1993;74(5):863–873.
14. Quinones B, Riento K, Olkkonen VM, Hardy S, Bennett MK. Syntaxin 2 splice variants exhibit differential expression patterns, biochemical properties and subcellular localizations. *J Cell Sci.* 1999;112 (pt 23):4291–4304.
15. Hirai Y, Takebe K, Takashina M, Kobayashi S, Takeichi M. Epimorphin: a mesenchymal protein essential for epithelial morphogenesis. *Cell.* 1992;69(3):471–481.
16. Oka Y, Hirai Y. Inductive influences of epimorphin on endothelial cells in vitro. *Exp Cell Res.* 1996;222(1):189–198.
17. Hirai Y, et al. Non-classical export of epimorphin and its adhesion to alphav-integrin in regulation of epithelial morphogenesis. *J Cell Sci.* 2007;120(pt 12):2032–2043.
18. Fritsch C, et al. Epimorphin expression in intestinal myofibroblasts induces epithelial morphogenesis. *J Clin Invest.* 2002;110(11):1629–1641.
19. Wang Y, et al. Epimorphin^{-/-} mice have increased intestinal growth, decreased susceptibility to dextran sodium sulfate colitis, and impaired spermatogenesis. *J Clin Invest.* 2006;116(6):1535–1546.
20. Feagins LA, Souza RF, Spechler SJ. Carcinogenesis in IBD: potential targets for the prevention of colorectal cancer. *Nat Rev Gastroenterol Hepatol.* 2009;6(5):297–305.
21. Greten FR, et al. IKKbeta links inflammation and tumorigenesis in a mouse model of colitis-associated cancer. *Cell.* 2004;118(3):285–296.
22. Neufert C, Becker C, Neurath MF. An inducible mouse model of colon carcinogenesis for the analysis of sporadic and inflammation-driven tumor progression. *Nat Protoc.* 2007;2(8):1998–2004.
23. Andoh A, Fujino S, Hirai Y, Fujiyama Y. Epimorphin expression in human colonic myofibroblasts. *Int J Mol Med.* 2004;13(1):57–61.
24. Plateroti M, et al. Subepithelial fibroblast cell lines from different levels of gut axis display regional characteristics. *Am J Physiol.* 1998;274(5 pt 1):G945–G954.
25. Yang YP, Klingensmith J. Roles of organizer factors and BMP antagonism in mammalian forebrain establishment. *Dev Biol.* 2006;296(2):458–475.
26. van Dop WA, et al. Depletion of the colonic epithelial precursor cell compartment upon conditional activation of the Hedgehog pathway. *Gastroenterology.* 2009;136(7):2195–2203.
27. Batts LE, Polk DB, Dubois RN, Kulessa H. Bmp signaling is required for intestinal growth and morphogenesis. *Dev Dyn.* 2006;235(6):1563–1570.
28. Haramis AP, et al. De novo crypt formation and juvenile polyposis on BMP inhibition in mouse intestine. *Science.* 2004;303(5664):1684–1686.
29. He XC, et al. BMP signaling inhibits intestinal stem cell self-renewal through suppression of Wnt-beta-catenin signaling. *Nat Genet.* 2004;36(10):1117–1121.
30. Fiocchi C. Intestinal inflammation: a complex interplay of immune and nonimmune cell interactions. *Am J Physiol.* 1997;273(4 pt 1):G769–G775.
31. Grivennikov S, et al. IL-6 and Stat3 are required for survival of intestinal epithelial cells and development of colitis-associated cancer. *Cancer Cell.* 2009;15(2):103–113.
32. Rigby RJ, Simmons JG, Greenhalgh CJ, Alexander WS, Lund PK. Suppressor of cytokine signaling 3 (SOCS3) limits damage-induced crypt hyper-proliferation and inflammation-associated tumorigenesis in the colon. *Oncogene.* 2007;26(33):4833–4841.
33. Hackam DJ, Rotstein OD, Bennett MK, Klip A, Grinstein S, Manolson MF. Characterization and subcellular localization of target membrane soluble NSF attachment protein receptors (t-SNAREs) in macrophages. Syntaxins 2, 3, and 4 are present on phagosomal membranes. *J Immunol.* 1996;156(11):4377–4383.
34. Andou A, et al. Dietary histidine ameliorates murine colitis by inhibition of proinflammatory cytokine production from macrophages. *Gastroenterology.* 2009;136(2):564–574; e562.
35. Kure I, et al. Lipoxin A4 reduces lipopolysaccharide-induced inflammation in macrophages and intestinal epithelial cells through inhibition of NF- κ B activation. *J Pharmacol Exp Ther.* 2010;332(2):541–548.
36. Zhang X, Goncalves R, Mosser DM. The isolation and characterization of murine macrophages. *Curr Protoc Immunol.* 2008;Chapter 14:Unit 14.1.
37. Teng FY, Wang Y, Tang BL. The syntaxins. *Genome Biol.* 2001;2(11):REVIEWS3012.
38. Zuber C, Fan JY, Guhl B, Roth J. Misfolded proinsulin accumulates in expanded pre-Golgi intermediates and endoplasmic reticulum subdomains in pancreatic beta cells of Akita mice. *FASEB J.* 2004;18(7):917–919.
39. Okunade GW, et al. Loss of the Atp2c1 secretory pathway Ca(2+)-ATPase (SPCA1) in mice causes Golgi stress, apoptosis, and midgestational death in homozygous embryos and squamous cell tumors in adult heterozygotes. *J Biol Chem.* 2007;282(36):26517–26527.
40. Marciniak SJ, Ron D. Endoplasmic reticulum stress signaling in disease. *Physiol Rev.* 2006;86(4):1133–1149.
41. Parkin CA, Ingham PW. The adventures of Sonic Hedgehog in development and repair. I. Hedgehog signaling in gastrointestinal development and disease. *Am J Physiol Gastrointest Liver Physiol.* 2008;294(2):G363–G367.
42. Madison BB, Braunstein K, Kuizon E, Portman K, Qiao XT, Gumucio DL. Epithelial hedgehog signals pattern the intestinal crypt-villus axis. *Development.* 2005;132(2):279–289.
43. Lees C, Howie S, Sartor RB, Satsangi J. The hedgehog signalling pathway in the gastrointestinal tract: implications for development, homeostasis, and disease. *Gastroenterology.* 2005;129(5):1696–1710.
44. Cohen MM Jr. The hedgehog signaling network. *Am J Med Genet A.* 2003;123A(1):5–28.
45. Nakamura T, Tsuchiya K, Watanabe M. Crosstalk between Wnt and Notch signaling in intestinal epithelial cell fate decision. *J Gastroenterol.* 2007;42(9):705–710.
46. van den Brink GR, et al. Indian Hedgehog is an antagonist of Wnt signaling in colonic epithelial cell differentiation. *Nat Genet.* 2004;36(3):277–282.
47. Clarke AR. Wnt signalling in the mouse intestine. *Oncogene.* 2006;25(57):7512–7521.
48. Blanpain C, Horsley V, Fuchs E. Epithelial stem cells: turning over new leaves. *Cell.* 2007;128(3):445–458.
49. Kosinski C, et al. Gene expression patterns of human colon tops and basal crypts and BMP antagonists as intestinal stem cell niche factors. *Proc Natl Acad Sci U S A.* 2007;104(39):15418–15423.
50. Ng SS, et al. Phosphatidylinositol 3-kinase signaling does not activate the wnt cascade. *J Biol Chem.* 2009;284(51):35308–35313.
51. Howe JR, et al. Germline mutations of the gene encoding bone morphogenetic protein receptor 1A in juvenile polyposis. *Nat Genet.* 2001;28(2):184–187.
52. Zhang Q, et al. Tumor-like stem cells derived from human keloid are governed by the inflammatory niche devoid by IL-17/IL-6 axis. *PLoS One.* 2009;4(11):e7798.
53. Becker C, et al. TGF-beta suppresses tumor progression in colon cancer by inhibition of IL-6 trans-signaling. *Immunity.* 2004;21(4):491–501.
54. Rosenberg DW, Giardina C, Tanaka T. Mouse models for the study of colon carcinogenesis. *Carcinogenesis.* 2009;30(2):183–196.
55. Gregorieff A, Pinto D, Begthel H, Destree O, Kielman M, Clevers H. Expression pattern of Wnt signaling components in the adult intestine. *Gastroenterology.* 2005;129(2):626–638.
56. Powell DW, Adegboyega PA, Di Mari JF, Mifflin RC. Epithelial cells and their neighbors I. Role of intestinal myofibroblasts in development, repair, and cancer. *Am J Physiol Gastrointest Liver Physiol.* 2005;289(1):G2–G7.
57. Boivin GP, et al. Pathology of mouse models of intestinal cancer: consensus report and recommendations. *Gastroenterology.* 2003;124(3):762–777.
58. Tang Y, Swartz-Basile DA, Swietlicki EA, Yi L, Rubin DC, Levin MS. Bax is required for resection-induced changes in apoptosis, proliferation, and members of the extrinsic cell death pathways. *Gastroenterology.* 2004;126(1):220–230.
59. Evans GS, Flint N, Somers AS, Eyden B, Potten CS. The development of a method for the preparation of rat intestinal epithelial cell primary cultures. *J Cell Sci.* 1992;101(pt 1):219–231.
60. Newberry RD, McDonough JS, McDonald KG, Lorenz RG. Postgestational lymphotoxin/lymphotoxin beta receptor interactions are essential for the presence of intestinal B lymphocytes. *J Immunol.* 2002;168(10):4988–4997.
61. Inaba K, Swiggard WJ, Steinman RM, Romani N, Schuler G, Brinster C. Isolation of dendritic cells. *Curr Protoc Immunol.* 2009;Chapter 3:Unit 3.7.